Journal of Materials Science: Materials in Electronics (2019) 30:16695–16701
https://doi.org/10.1007/s10854-019-01496-6

REVIEW

Thermal, structural and optical properties of TeO_2–Na_2O–TiO_2 glassy system

Jaqueline Valeski Gunha[1] · Anderson Gonçalves[1,2] · Aloisi Somer[1] · André Vitor Chaves de Andrade[1] · Daniele Toniolo Dias[3] · Andressa Novatski[1]

Received: 27 February 2019 / Accepted: 8 May 2019 / Published online: 14 May 2019

Abstract
In this work, $80TeO_2$–$(20-x)$ Na_2O–$xTiO_2$ (x = 0, 5, 10 and 20) mol% glasses by melting quenching technique were obtained. Density (ρ) and molar volume (V_m) of these glasses have been investigated. The characterization was performed by X-ray diffraction (XRD), differential scanning calorimetry (DSC), Fourier transform infrared (FTIR) and ultraviolet–visible (UV–Vis) spectroscopy. As expected, the V_m values decreased with x increasing, exhibiting a density opposite behavior. DSC, FTIR and UV–Vis results indicated that, with the increasing the TiO_2 content, the role of this oxide changes from network modifier to former. In addition, more covalent bonds are formed, reinforcing the network connectivity by increasing the Te–O–Ti inter-chain bounds. These features improved the glassy system thermal and optical properties.

1 Introduction

TeO_2-based glasses have increasing scientific and technological interest due to wide optical transmission window (0.350 to 5.0 μm), consistent vitreous stability ($\Delta T > 100\ cm^{-1}$) and low phonon energy (between 600 to 850 cm^{-1}) [1–3]. Additionally, these materials behold density over 4 g/cm^{-3} and linear refractive index higher than 2 [4–6]. These properties allows application for photonics and electronics, such as: optical fiber, amplifiers and sensors [2, 7, 8].

The TeO_2-glassy is obtained only with ultra-rapid cooling rates [9]. However, the addition of modifier oxides, such as alkali, alkaline earth or transition metal oxides drops the cooling rates to 1 kJ/s, making it possible to obtain these glasses by conventional melt-quenching technique [10–13].

The addition of Na_2O in TeO_2-based glasses was first reported by Mochida et al. with a range of glass formation between $10 \leq x \leq 46.5$ mol% [11]. The Na_2O oxide plays the role of network modifier, causing the transformation of the basic structural unit TeO_4 to TeO_{3+1}, breaking the Te–O–Te linkages [14]. Nishida et al. [15] proposed that this transformation occurs due to the change of the glass matrix from a three- or two-dimensional network structure to a lower dimensional one. These structural changes gives rise to consequences on the thermal properties decreasing the vitreous transition temperature (T_g) [3, 16].

On the other hand, TiO_2 is effective in reinforce TeO_2 glass network by the substitutional positioning of Te to Ti site [6, 17, 18]. In addition, the incorporation of this oxide increases third-order optical non-linearities, linear refractive index and thermal stability for systems like TeO_2–Li_2O–TiO_2. These features have been attributed to the change in coordination from TeO_3 to TeO_4 units by Te–O–Ti linkages [4, 19–22].

In this sense, the correlation between structural with thermal and optical properties of TeO_2–Na_2O–TiO_2 glassy system were investigated, in order to understand the role of TiO_2 into the glass as Na_2O was exchanged for TiO_2.

2 Materials and methods

The $80TeO_2$–$(20-x)$ Na_2O–$xTiO_2$ (x = 0, 5, 10, 15 and 20 mol%) samples were prepared by means of melt-quenching technique in air atmosphere. The precursors reagents: TeO_2 (Alfa Aesar 99.99%), Na_2O (Sigma-Aldrich 99.5%)

✉ Jaqueline Valeski Gunha
jaquegunha@gmail.com

[1] Departamento de Física, Universidade Estadual de Ponta Grossa, Ponta Grossa, PR 84016-210, Brazil

[2] Departamento de Física, Universidade Estadual de Maringá, Maringá, PR 87020-900, Brazil

[3] Departamento Acadêmico de Física, Universidade Tecnológica Federal do Paraná, Ponta Grossa, PR 87030-900, Brazil

and TiO_2 (Synth 99.5%) were weighted and mixed with pistil and agate mortar during 40 min. The mixtures were melted in Pt crucible at a temperature of 840 °C for 30 min. The melt was quenched in a preheated brass mold at a temperature 20 °C lower than T_g and submitted to an annealing treatment for 240 min.

The density measurements were carried out by means the Archimedes's Principle with xylene ($\rho = 0.88$ g/cm$^{3)}$ using a balance (AY220, Shimadzu) with 10^{-4} g precision. The diffractograms were recorded on X-ray Automatic Diffractometer (Ultima IV, Rigaku) at a scan rate of 2°/min (CuKα radiation $\lambda = 1.5418$ Å, 30 kV, 40 mA).

Differential Scanning Calorimetry (DSC) data were obtained with a 4 °C precision in calorimeter (Labsys Evo, Setaram Instrumentation). Such measures were realized under Argon atmosphere with 20 mL/min flux and heating rate of 10 °C/min, from ambient temperature to 600 °C using alumina crucible. In order to apply DRX and DSC, the samples were powdered and sieved (≤ 53 µm).

The structural analysis was carried out by means of Fourier transform infrared (FTIR) spectroscopy. For FTIR it was used a spectrometer, (IR-Prestige 21, Shimadzu). The glassy powdered samples were pulverized in an agate mortar with 100 mg of KBr in the 1:50 proportion. The resulting spectra were obtained in the absorbance model in the interval between 4000 and 400 cm^{-1} using 64 scans with 4 cm^{-1} resolution.

The optical absorption spectra were acquired using a spectrometer (Carry 50, Varian) in the wavelength range 300–700 nm. The samples thickness were 300 µm.

3 Results and discussion

3.1 Density, molar volume and oxygen density packing

The physical parameters density (ρ), molar volume (V_m) and oxygen density package (OPD) are presented in Table 1. The ρ values observed in samples for x = 0 and x = 20 corroborate with the previously reported [23, 24]. The exchange of Na_2O by TiO_2 increases the ρ values, which is due to the substitution of a lower molecular weight substance (Na_2O 61.98 g/mol) with a higher molecular weight one (TiO_2 79.87 g/mol), resulting in an increase in total molecular weight. Besides, the density increase is due to the structural modifications occurring in the amorphous network. In sample with x = 0, Na_2O plays the role of network modifier changing the Te atom coordination from $TeO_4 \rightarrow TeO_3$. With TiO_2 addition, more covalent bonds are formed, promoting a continuous glassy network by the Te–O–Ti linkages [17].

Other physical parameters which can contribute with valuable information about the changes in glass structure are molar volume and the oxygen packing density. V_m was calculated by using $V_m = \frac{M}{\rho}$, where M is the glass sample molecular weight. The OPD was determined using the equation: $OPD = 1000C_0 \times \frac{\rho}{M}$, where C_0 is the number of oxygen atoms per formula unit. As expected, the V_m values (Table 1) decrease from 29.1 to 27.26 cm^3/mol, with increasing x, exhibiting density opposite behavior. The increase of OPD values (Table 1) with x is an indicative of close packing glass network structure. This packing degree is dependent of cation field intensity and the cation radius [25]. Since the ionic radius of Na^+ and Ti^{4+} are 0.098 nm and 0.064 nm, respectively [26]. Therefore, the average of the cation field intensity increases with x, consequently increasing the OPD.

3.2 X-ray diffraction (XRD) results

Figure 1 presents the XRD results of the studied samples. We can notice that the sample in the composition for x = 0 is mostly amorphous, except for two sharp peaks at 13.3 and 26.5° superimposed on broad peaks due to the majority glassy phase. In fact, during the experimental studies, this sample was observed to be hygroscopic, such behavior is in accordance with literature for $(100-x)TeO_2$–xNa_2O binary system. This feature can be attributed to the hydrated compound presence such as $Na_2Te_2O_5{\cdot}2H_2O$ phase [23]. For x = 5 we notice the predominant amorphous character with some sharp peaks superimposed at 13.3 and 26.5°, showing the same $Na_2Te_2O_5$ phase presence. The peaks at 26.1, 29.8 and 32.0° are attributed to the $TiTe_3O_8$ phase [27]. The αTeO_2 phase presents peaks at 28.7 and 48.5°. For x = 10 and x = 15 the samples presented amorphous character. The sample with x = 20 contained significant amount of crystalline phases and presented several

Table 1 Values of: density (ρ); molar volume (V_m); oxygen packing density (OPD); glass transition (T_g); onset crystallization (T_x); peak crystallization (T_c); thermal stability (ΔT); and parameter Weinberg (H_w)

Sample	ρ (g/cm^3)	V_m (cm^3/mol)	OPD (mol/L)	T_g (°C) ±2	T_x (°C) ±2	T_c (°C) ±2	ΔT (°C) ±2	H_w
x = 0	4.81 ± 0.04	29.1 ± 0.2	61.9 ± 0.5	245	348	370	103	0.42 ± 0.01
x = 05	4.97 ± 0.02	28.4 ± 0.1	65.2 ± 0.3	272	321	340	49	0.18 ± 0.01
x = 10	5.09 ± 0.01	27.88 ± 0.05	68.2 ± 0.1	302	358	375	56	0.19 ± 0.01
x = 15	5.16 ± 0.03	27.7 ± 0.1	70.4 ± 0.4	348	408	441	60	0.17 ± 0.01
x = 20	5.27 ± 0.01	27.26 ± 0.05	73.3 ± 0.1	367	411	442	44	0.12 ± 0.01

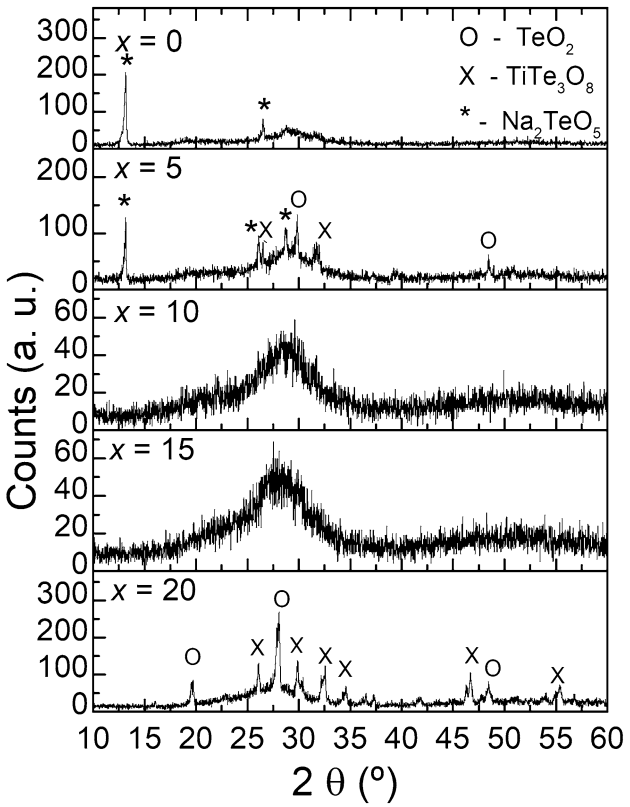

Fig. 1 Diffractograms indicating the different phases formed in x = 20, 15 and 0 samples

peaks attributed αTeO_2 (19.7, 28.7 and 48.5°) and $TiTe_3O_8$ (26.1, 29.8, 32.0, 34.6, 46.7 and 55.4°) [28].

Figure 2 shows, the all sample photo that were characterized in Fig. 1. These samples change from yellowish to brownish with increasing x, being the glassy sample (x = 10 and x = 15) and partially crystallized (x = 0, 5 and 20).

3.3 Differential scanning calorimetry (DSC) results

Thermal behavior of each sample was determined by DSC analysis. The obtained thermograms are presented in Fig. 3. From these data, the glass transition (T_g), the onset crystallization (T_x), the first exothermic peak at the crystallization (T_c) temperatures and the thermal stability were determined. The last one was determined using two criteria: $\Delta T = T_x - T_g$, which is frequently used for glass materials, and the Weinberg parameter $H_w = \frac{T_x - T_g}{T_g}$ [29, 30]. These results are presented in Table 1. We can notice an increase in T_g from 245 to 367 °C with the exchange of Na_2O for TiO_2. This increase can be related to the reinforcement of the glass network due to the high coordination number of Ti^{4+} (4 or 6) [31]. Besides, the asymmetric crystallization peak for x = 0, 5 and 20 suggests different distinct phase crystallizations. The shift in T_c from 370 to 340 °C with x = 5 is an indicator of the increasing concentration of nuclei in the glass and consequently the probability of crystallization inside the glass matrix increases, this is a direct consequence of the αTeO2 presence, as observed in XRD results [32].

In binary glasses, excessive addition of a network modifier decreases vitrification behavior, due to the decreasing stability of TeO_3 units [23], increasing T_g values and decreasing glass-forming ability. So, the addition of 5% mol of TiO_2 makes this oxide plays a role of modifier network. However, for 10 and 15% mol the TiO_2 assumes the role of former network, rearranging the breaking caused by Na_2O which creates TeO_3 and TeO_{3+1} and does not allow the formation of the $Na_2Te_2O_5$ phase, facilitating the amorphization of the glass network. This directly impacts the shape of the peak T_c which is narrower for the samples x = 10 and 15 and is shifted to higher temperatures, indicating a lower concentration of nuclei that induce the crystallization.

In Table 1, ΔT decreases from x = 0 to x = 5 and slightly increases for x = 10 and 15. This behavior is in accordance with XRD results, since the samples x = 10 and 15 presented an amorphous behavior showing that the melting quenching technique was successfully performed for these two compositions. This result endorses the change of the role of TiO_2 oxide from network modifier to former. Besides, H_w (Table 1) decreases with the exchange of Na_2O for TiO_2, that suggest an increase in the crystallization tendency [33] which is an indicator of the substitution of Te–O–Te for Te–O–Ti bounds favoring the covalent character of the network [34]. These statements are reinforced by ρ, V_m and OPD results.

3.4 FTIR analysis

In order to obtain some insights about the structural change with composition, FTIR experiments were performed and the results are shown in Fig. 4. According to the literature, in the region from 400 to 1000 cm^{-1}, there are, at least, eight characteristic regions corresponding to the different structural units present in tellurite glasses with TiO_2: ~450, 580, 620, 660, 710, 750, 780, 800–830, 852–890. [22, 23, 27, 32, 35–38].

The region at ~450 cm^{-1} can be related to Te–O–Te and/or Te–O–Ti stretching vibrations. Besides, for x = 0 we notice a shoulder at 451 cm^{-1} and for x = 20 at 440 cm^{-1}.

Fig. 2 Samples photograph in bulk after melting quenching

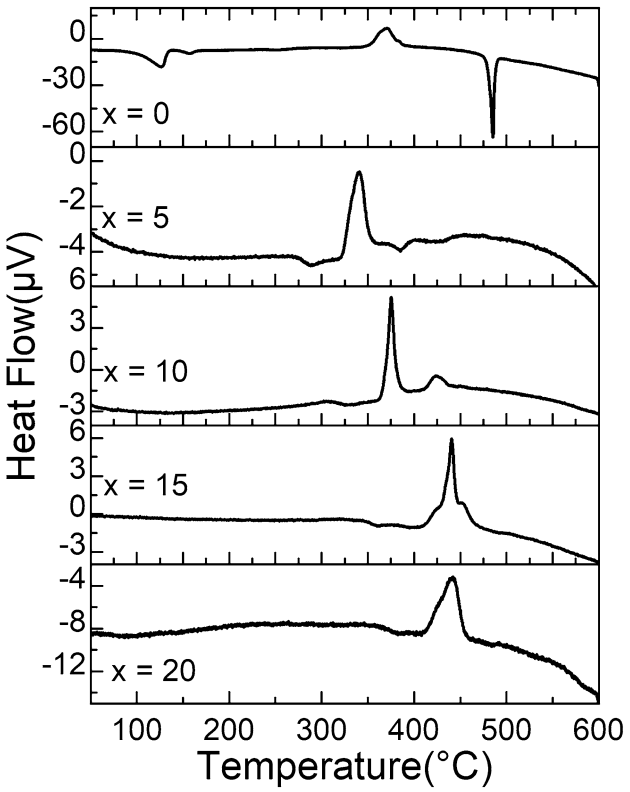

Fig. 3 DSC scans of samples

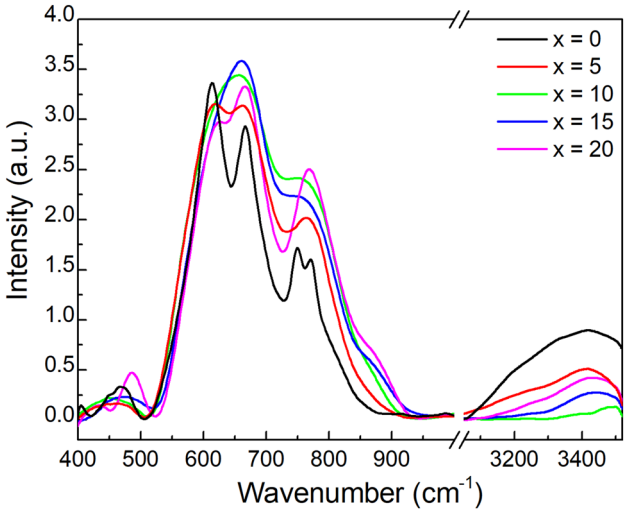

Fig. 4 FTIR spectra of samples

This shoulder has been related to symmetric stretching of O–Te–O in α-TeO_2 structure. The 467 cm^{-1} peak for x = 0 is related to Te–O–Te stretching vibrations. For x = 20, Te–O–Ti stretching vibrations appear at 486 cm^{-1}. For x = 5, 10 and 15 these modes were superimposed and presented a broad band in this region [27, 32, 35].

The region at 2900 - 3500 cm^{-1} is attributed to the vibration of the elongation of the hydroxyl group and hydrogen. This high intensity region decreases with increasing x. In this case the high Na_2O content confirm the sample tendency to be hygroscopic [36].

FTIR results in the region from 500 to 950 cm^{-1} were detailed into Gaussian fitting as presented in Fig. 5. The band centered at 580 cm^{-1}, which is attributed to Te–O stretching vibrations of TeO_4 and TeO_{3+1} units, remains at the same position but decreases in area from x = 10 to x = 20. According to Dimitriev [38], the addition of modifier network stimulates TeO_{3+1} units formation. Our results showed that the TiO_2 acts as network modifier for the sample with x = 5. On the other hand, for x = 10, 15 and 20 its role changed from network modifier to former reinforcing the DSC results as shown in Fig. 3.

The band area at 620 cm^{-1} increases with x content. This mode, which is attributed to Te–O bonds of deformed TeO_4 units, increases from x = 0 to x = 5, remains constant from x = 5 to x = 15 and increases to x = 20. This behavior is an indicative that TiO_2 inhibits the Na2O action in creates more TeO_{3+1} and TeO_3 from TeO_4 units [3, 23]. The 660 cm^{-1} band is associated to asymmetric stretching vibration of Te–O bonds in TeO_3 pyramidal units [3]. The intensity of this band remains approximately constant up to x = 15 and

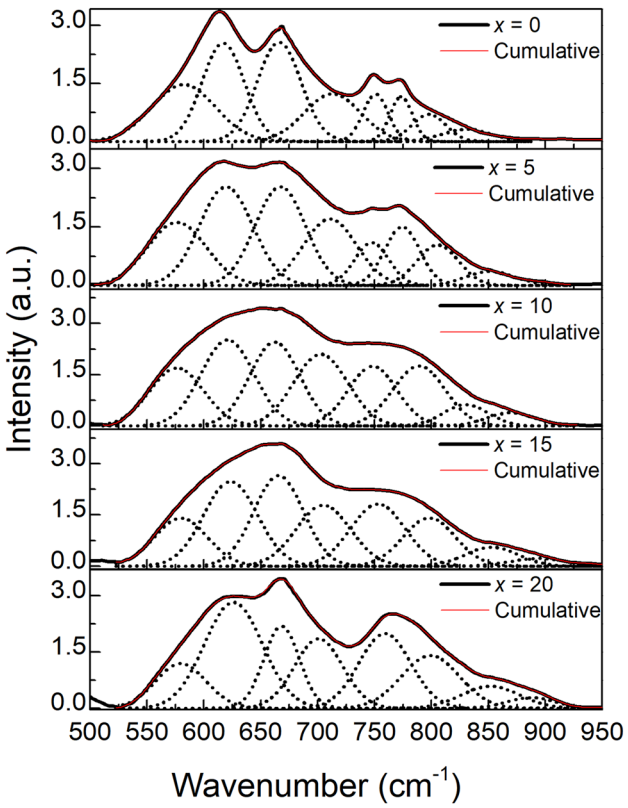

Fig. 5 Deconvoluted FTIR spectra of samples

decreases for x = 20. The 710 cm^{-1} band increases up to x = 10 and decreases with increasing x, this band can be attributed to TeO_3 units [38]. The band at 750 cm^{-1} is attributed to TeO_{3+1} unit and increases with x content. The band at 773 cm^{-1} is well resolved for x = 0 and x = 5 samples and it is attributed to αTeO_2 [36]. For the other samples this mode vibration is superimposed with the 800 cm^{-1} which it is attributed to TeO_3 units [23]. This band decrease in intensity increasing x content in the samples. In Fig. 5, shifts from 800 to 852 cm^{-1} and from 831 to 889 cm^{-1}, with x increasing from 5 to 20 can be perceived. These bands are related to stretching vibration of Ti–O–Ti bridges in TiO_4 units [36]. FTIR analyses indicate that when Ti is incorporated in Te–O–Te interchain, Te–O–Ti bonds are formed, and for relative high TiO_2 composition and after a saturation of Te–O–Ti interchains, occurs the TiO_4 units formation [22, 23, 27, 35, 36].

3.5 Optical absorption

The analysis of the optical absorption edge is useful to obtain some insights about the optical transition and optical bandgap of materials. According to the literature [39], in glasses, the UV absorption edge shifts to longer wavelengths by increasing the molecular weight of their precursor oxides. The yellow color of the glasses, as observed in Fig. 2, is due to a variable shift of the ultraviolet absorption edge towards the visible range, which depends on the glass composition. For the analyzed samples, it was not possible to analyze the x = 20 sample UV edge, since it was completely opaque even for 300 μm thickness. For the other samples, the optical band gap and Urbach´s energy were determined.

Davis and Mott [40] presented an expression for the absorption coefficient (α) as a function of photon energy (hν), as follow:

$$\alpha(h\upsilon) \propto \left(h\upsilon - E_G\right)^m \quad (1)$$

where α is the absorption coefficient, (hν) is the energy of the photon, E_g is the bandgap energy and *m* indicates the type of electronic transition involved in the absorption process. The values for *m* depend on the bandgap characteristic: m = 1/2 for direct allowed transition; m = 3/2 for direct forbidden transition, m = 2 for indirect allowed transition and m = 3 for indirect forbidden transition. The absorption spectra presented in Fig. 6a were used to determine the optical bandgap (E_g) of samples using Eq. 1. Figure 6b presents the curves of $(\alpha.h\nu)^{1/m}$ versus photon energy, with the E_g values being estimated by extrapolation of the linear portion of the curves, where $(\alpha.h\nu)^{1/m} = 0$. The best fit was obtained for m = 2, indicating an indirect allowed transition [41]. Another method to determine the bandgap is the intersection point between lines that extrapolate absorption coefficient values

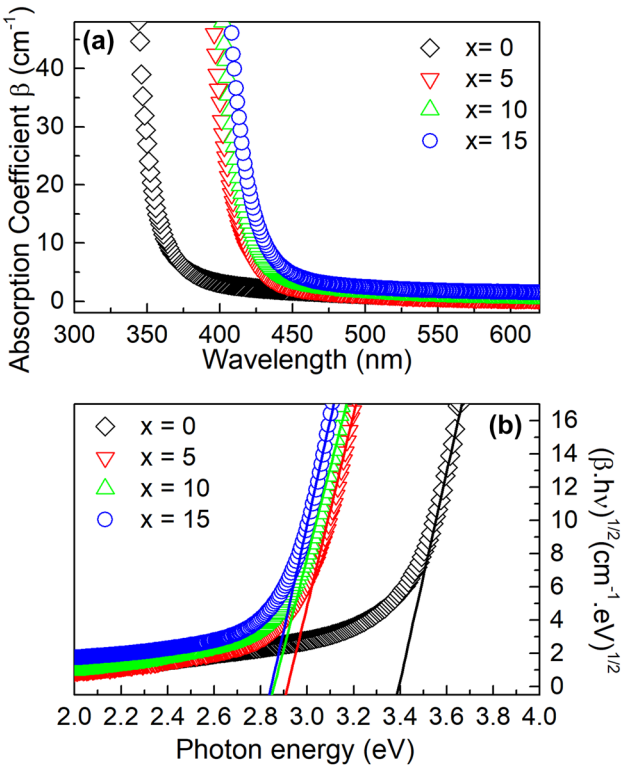

Fig. 6 **a** Optical absorption spectra of the studied glasses. **b** $(\alpha.h\nu)^{1/2}$ versus photon energy showing the linear regression for E_g determination

Table 2 Bandgap values (E_g and E'_g), Urbach's energy (ΔE), and electronic ion polarizability of the samples

Sample	E_g (eV) (±0.003)	$E_{g'}$ (eV)	ΔE (eV) (±0.004)	$\gamma^2_O(E_g)$ Å^3
x = 0	3.394	3.46	0.488	3.02 ± 0.03
x = 5	2.915	2.99	0.171	3.04 ± 0.01
x = 10	2.857	2.93	0.185	2.922 ± 0.007
x = 15	2.845	2.89	0.198	2.831 ± 0.006

in the small hν range and at the linear absorption edge $\left(E'_g\right)$ [42]. Table 2 presents the values of E_g and E'_g in eV. The E_g values changes from 3.394 to 2.845 eV with increasing *x* content. In principle, this behavior would be related to the increase in defects of glassy network, however from FTIR and DSC results we noticed that the exchange of Na_2O for TiO_2 is reinforcing the network. In fact, this behavior can be explained by means of ion oxide polarizability and it will be discussed later.

The optical absorption coefficient near the fundamental absorption band has an exponential dependency, which is given by the Urbach´s rule [41]:

$$\alpha = \alpha_0 \exp\left(\frac{h\nu}{\Delta E}\right) \quad (2)$$

in which α_0 is a constant and ΔE is the Urbach's energy. ΔE corresponds to the optical transitions between localized tail states adjacent to the valence band and extended states in the conduction band above the mobility edge [43]. The absorption coefficient values (in log scale) were plotted against the photon energies. The ΔE values were obtained by linear fitting from those plots and are presented in Table 2. It can be notice that the ΔE values decrease and then increase from x = 5 to x = 15. According to Mott and Davis [40] model, this energy depends on the degree of the both disorder and defects of the amorphous structure. If the glass has a more polymerized network, Urbach´s energy is lower.

According to the literature [43], the behavior of the polarizability of the electronic ion are calculated by the following Eq. 3:

$$\gamma_{O^{2-}}(E_g) = \left[\left(\frac{V_m}{2,52}\right)\left(1-\sqrt{\frac{E_g}{20}}\right) - \sum p\gamma_i\right](q)^{-1} \quad (3)$$

were γ is a polarizability of the cation, V_m is the molar volume, p denotes the number of cations and q oxide ions respectively, in de chemical formula $A_p O_q$. Figure 7 presents the bandgap values (E_g), Urbach's energy (ΔE), and the polarizability (γ_O^2) versus TiO_2 content.

The polarizability behavior should be inverse to the bandgap; however, this behavior does not occur to our system. The substitution of Na_2O by TiO_2 generated a decrease in the bandgap, but there is a polarizability atypical behavior, which does not accompany inversely the bandgap.

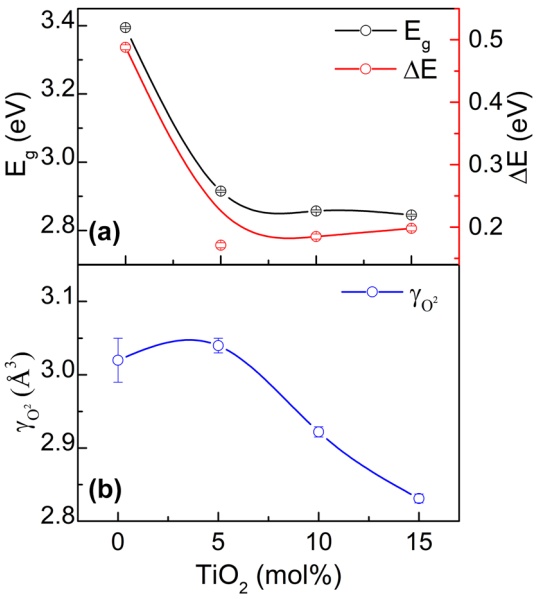

Fig. 7 **a** Bandgap and ΔE energy values and **b** polarizability values γ_{02} versus TiO_2 content

Therefore, this same behavior which decreases the polarizability is related to the increase of mean simple bonding [43, 44]. This increase in average simple bonding is observed when a certain amount of TiO_2 added, suggesting that there is an *onset* of composition which allow the formation of strong chemical bonds in the glass network. This statement is reinforced by the DSC results, which show a decrease in thermal stability for the samples. Finally, the feature of changing the role of TiO_2 from network modifier to former drastically influences the thermal and optical properties in TeO_2–Na_2O–TiO_2 glassy system.

4 Conclusion

We conclude that the structural of the TeO_2–Na_2O–TiO_2 system investigated by FTIR analysis, with the equimolar substitution of Na_2O by TiO_2 showed a structural transformation in the TeO2 network. The Na_2O performs the role of network modifier, changing the coordination of the atom of $TeO_4 \rightarrow TeO_3$. With the addition of TiO_2, more covalent bonds are formed, promoting a continuous glass network through the Te–O–Ti bond. The XRD results corroborate with FTIR, and the presence of the hydrated compound, such as the $Na_2Te_2O_5{\cdot}2H_2O$ phase and the $TiTe_3O_8$ phase.

In addition, the decrease in polarization is related to the increase in the mean simple bonding. This strong bond increase, which is related to decreases of the bandgap and polarizability values, indicates the increase of Te–O–Ti bonds (band at 450 cm^{-1}). This increase also agrees with the DSC results, which show a decrease in the thermal stability for the samples. Finally, we conclude that TiO_2 changes its role from network modifier to former after 5 mol%, which drastically influences the thermal and optical properties through increasing the network connectivity.

Acknowledgments The authors thank to FINEP, CAPES, CNPQ and Fundação Araucária for the partial financial support. To LABMU-UEPG for technical support.

References

1. H. Bürger, W. Vogel, V. Kozhukharov, IR transmission and properties of glasses in the TeO_2–RnOm, RnXm, Rn (SO_4) m, Rn (PO_3) mandB_2O_3] systems. Infrared Phys. **25**, 395–409 (1985)
2. J.S. Wang, E.M. Vogel, E. Snitzer, Tellurite glass: a new candidate for fiber devices. Opt. Mater. (Amst) **3**, 187–203 (1994)
3. J. Heo, D. Lam, G.H. Sigel Jr., E.A. Mendoza, D.A. Hensley, Spectroscopic analysis of the structure and properties of alkali tellurite glasses. J. Am. Ceram. Soc. **75**, 277–281 (1992)
4. F. Chen, T. Xu, S. Dai, Q. Nie, X. Shen, J. Zhang, X. Wang, Linear and non-linear characteristics of tellurite glasses within TeO_2–Bi_2O_3–TiO_2 ternary system. Opt. Mater. (Amst) **32**, 868–872 (2010)

5. H. Takebe, S. Pujino, K. Morinaga, Refractive-index dispersion of tellurite glasses in the region from 0.40 to 1.71 μm. J. Am. Ceram. Soc. **77**, 2455–2457 (1994)
6. M. Udovic, P. Thomas, A. Mirgorodsky, O. Durand, M. Soulis, O. Masson, T. Merle-Méjean, J.-C. Champarnaud-Mesjard, Thermal characteristics, Raman spectra and structural properties of new tellurite glasses within the Bi_2O_3–TiO_2–TeO_2 system. J. Solid State Chem. **179**, 3252–3259 (2006)
7. N. Boubata, A. Roula, I. Moussaoui, Thermodynamic and relative approach to compute glass-forming ability of oxides. Bull. Mater. Sci. **36**, 457–460 (2013)
8. S. Manning, H. Ebendorff-Heidepriem, T.M. Monro, Ternary tellurite glasses for the fabrication of nonlinear optical fibres. Opt. Mater. Express. **2**, 140–152 (2012)
9. P.T. Sarjeant, R. Roy, New glassy and polymorphic oxide phases using rapid quenching techniques. J. Am. Ceram. Soc. **50**, 500–503 (1967)
10. R. El-Mallawany, The optical properties of tellurite glasses. J. Appl. Phys. **72**, 1774–1777 (1992)
11. N. Mochida, K. Takahashi, K. Nakata, S. Shibusawa, Properties and structure of the binary tellurite glasses containing mono-and di-valent cations. J. Ceram. Assoc. Jpn. **86**, 317–326 (1978)
12. H. Bürger, K. Kneipp, H. Hobert, W. Vogel, V. Kozhukharov, S. Neov, Glass formation, properties and structure of glasses in the TeO_2–ZnO system. J. Non. Cryst. Solids. **151**, 134–142 (1992)
13. D. Souri, Y. Shahmoradi, Calorimetric analysis of non-crystalline TeO_2–V_2O_5–Sb_2O_3. J. Therm. Anal. Calorim. **129**, 601–607 (2017)
14. T. Sekiya, N. Mochida, A. Ohtsuka, M. Tonokawa, Raman spectra of $MO_1/2TeO_2$ (M = Li, Na, K, Rb, Cs and Tl) glasses. J. Non. Cryst. Solids. **144**, 128–144 (1992)
15. T. Nishida, S. Saruwatari, Y. Takashima, Structural study of Na_2O–TeO_2 glasses by Mössbauer spectroscopy and differential thermal analysis. Bull. Chem. Soc. Jpn **61**, 4093–4097 (1988)
16. Y. Himei, A. Osaka, T. Nanba, Y. Miura, Coordination change of Te atoms in binary tellurite glasses. J. Non. Cryst. Solids. **177**, 164–169 (1994)
17. T. Hayakawa, M. Koduka, M. Nogami, J.R. Duclère, A.P. Mirgorodsky, P. Thomas, Metal oxide doping effects on Raman spectra and third-order nonlinear susceptibilities of thallium–tellurite glasses. Scr. Mater. **62**, 806–809 (2010)
18. M. Soulis, A.P. Mirgorodsky, T. Merle-Méjean, O. Masson, P. Thomas, M. Udovic, The role of modifier's cation valence in structural properties of TeO_2-based glasses. J. Non. Cryst. Solids. **354**, 143–149 (2008)
19. S.M. Lima, W.F. Falco, E.S. Bannwart, L.H. Andrade, R.C. Oliveira, J.C.S. Moraes, K. Yukimitu, E.B. Araújo, E.A. Falcão, A. Steimacher et al., Thermo-optical characterization of tellurite glasses by thermal lens, thermal relaxation calorimetry and interferometric methods. J. Non. Cryst. Solids. **352**, 3603–3607 (2006)
20. H. Nasu, O. Matsushita, K. Kamiya, H. Kobayashi, K. Kubodera, Third harmonic generation from Li_2O–TiO_2–TeO_2 glasses. J. Non. Cryst. Solids. **124**, 275–277 (1990)
21. W.A. Capanema, K. Yukimitu, J.C.S. Moraes, F.A. Santos, M.S. Figueiredo, S.M. Sidel, V.C.S. Reynoso, O.A. Sakai, A.N. Medina, The structure and optical dispersion of the refractive index of tellurite glass. Opt. Mater. (Amst) **33**, 1569–1572 (2011)
22. W. Stambouli, H. Elhouichet, M. Ferid, Study of thermal, structural and optical properties of tellurite glass with different TiO_2 composition. J. Mol. Struct. **1028**, 39–43 (2012)
23. K.B. Kavaklioğlu, S. Aydin, M. Çelikbilek, A.E. Ersundu, The TeO_2–Na_2O system: thermal behavior, structural properties, and phase equilibria. Int. J. Appl. Glas. Sci. **6**, 406–418 (2015). https://doi.org/10.1111/ijag.12103
24. G. Jayasinghe, D. Coppo, P. Bandaranayake, J.L. Souquet, Electrical properties of TeO_2 glasses with Na_2O as network modifier. Solid State Ionics **76**, 297–300 (1995)
25. A. Bachvarova-Nedelcheva, R. Iordanova, S. Ganev, Y. Dimitriev, Glass formation and structural studies of glasses in the TeO_2–ZnO–Bi_2O_3–Nb_2O_5 system. J. Non. Cryst. Solids. **503**, 224–231 (2019)
26. V. Dimitrov, T. Komatsu, An interpretation of optical properties of oxides and oxide glasses in terms of the electronic ion polarizability and average single bond strength. J. Univ. Chem. Technol. Met. **45**, 219–250 (2010)
27. I. Shaltout, Crystallization kinetics and structure of (TeO_2–TiO_2–Fe_2O_3) glasses. J. Mater. Sci. **35**, 323–329 (2000)
28. N. Elkhoshkhany, R. El-Mallawany, E. Syala, Mechanical and thermal properties of TeO_2–Bi_2O_3–V_2O_5–Na_2O–TiO_2 glass system. Ceram. Int. **42**, 19218–19224 (2016)
29. A.F. Kozmidis-Petrović, Theoretical analysis of relative changes of the Hruby, Weinberg, and Lu–Liu glass stability parameters with application on some oxide and chalcogenide glasses. Thermochim. Acta **499**, 54–60 (2010)
30. A.F. Kozmidis-Petrović, Sensitivity of the Hruby, Lu–Liu, Fan, Yuan, and Long glass stability parameters to the change of the ratios of characteristic temperatures Tx/Tg and Tm/Tg. Thermochim. Acta **510**, 137–143 (2010)
31. F. Chen, Q. Yu, B. Qiao, S. Dai, Q. Zhang, Influence of TiO_2 on thermal stability and crystallization kinetics of tellurite glasses within TeO_2–Bi_2O_3–Nb_2O_5 pseudo-ternary system. J. Non. Cryst. Solids. **404**, 32–36 (2014)
32. E. Idalgo, E.B. Araújo, K. Yukimitu, J.C.S. Moraes, V.C.S. Reynoso, C.L. Carvalho, Effects of the particle size and nucleation temperature on tellurite $20Li_2O$–$80TeO_2$ glass crystallization. Mater. Sci. Eng., A **434**, 13–18 (2006)
33. M.C. Weinberg, Assessment of glass stability criteria. Phys. Chem. Glas. **35**, 119–123 (1994)
34. J.-C. Sabadel, P. Armand, P.-E. Lippens, D. Cachau-Herreillat, E. Philippot, Mössbauer and XANES of TeO_2–BaO–TiO_2 glasses. J. Non Cryst. Solids. **244**, 143–150 (1999)
35. M. Çelikbilek, A. Erçin Ersundu, S. Aydin, Glass formation and characterization studies in the TeO_2–WO_3–Na_2O System. J. Am. Ceram. Soc. **96**, 1470–1476 (2013)
36. I.N. Sapian, M.I.M. Yusof, A.K. Yahya, Elastic and structural properties of (95–x) TeO_2-$5La_2O_3$-xTiO_2 lanthanum tellurite glass system. Chalcogenide Lett. **11**, 10 (2014)
37. S.Q. Mawlud, M.M. Ameena, M.R. Sahar, Z.A.S. Mahraz, K.F. Ahmed, Thermal stability and Judd-Ofelt analysis of optical properties of Sm3+-doped sodium tellurite glasses, in: AIP Conf. Proc., 2017: p. 20032
38. Y. Dimitriev, V. Dimitrov, M. Arnaudov, IR spectra and structures of tellurite glasses. J. Mater. Sci. **18**, 1353–1358 (1983)
39. M.A. Villegas, J.M.F. Navarro, Physical and structural properties of glasses in the TeO_2–TiO_2–Nb_2O_5 system. J. Eur. Ceram. Soc. **27**, 2715–2723 (2007)
40. E.A. Davis, N.F. Mott, Conduction in non-crystalline systems V. Conductivity, optical absorption and photoconductivity in amorphous semiconductors. Philos. Mag. **22**, 903–922 (1970)
41. F. Urbach, The long-wavelength edge of photographic sensitivity and of the electronic absorption of solids. Phys. Rev. **92**, 1324 (1953)
42. M. Nowak, B. Kauch, P. Szperlich, Determination of energy band gap of nanocrystalline SbSI using diffuse reflectance spectroscopy. Rev. Sci. Instrum. **80**, 46107 (2009)
43. V. Dimitrov, S. Sakka, Electronic oxide polarizability and optical basicity of simple oxides. J. Appl. Phys. **79**, 1736–1740 (1996)
44. V. Dimitrov, T. Komatsu, Classification of oxide glasses: a polarizability approach. J. Solid State Chem. **178**, 831–846 (2005)